Software Wave Receiver for the SS-520-2 Rocket Experiment

Kozo Hashimoto, *Senior Member, IEEE*, Hironori Iwai, Yoshikatsu Ueda, Hirotsugu Kojima, and
Hiroshi Matsumoto, *Fellow, IEEE*

Abstract—A software wave receiver was aboard the SS-520-2
rocket as a part of the plasma wave analyzer and successfully ac-
complished waveform observations and spectral observations. In
the present paper, we describe the specifications and roles of the
software wave receiver on the SS-520-2 rocket experiment. This
receiver consists of a waveform receiver using real-time data com-
pression and a spectral receiver with high time and frequency res-
olution using a programmable down converter. We report here on
the first flight test of the new plasma wave receiver to be used for
future planet explorers and space observation missions. Every 0.5
s, spectra of a 3-MHz signal with 0.3-kHz resolution are obtained,
and the data compression of waveforms with the bandwidth of 15
kHz are performed. Although the sweep time was occassionally af-
fected if the data were not compressed enough, no data were lost
during the flight.

Index Terms—Data compression, digital down converter, digital
sweep frequency receiver, plasma waves, software receiver,
SS-520-2 rocket experiment.

Fig. 1.   Block diagram of the PWA onboard SS-520-2 rocket [12].

I. INTRODUCTION

PLASMA wave observations from satellites are essential
for studying the wave–particle interactions in magneto-
spheres. On AKEBONO (EXOS-D), an auroral observation
satellite, the very low frequency (VLF) instruments [1], [2] were
designed to investigate the behavior of plasma waves associated
with auroral particles. They consisted of the wideband receiver
(WBA), multichannel analyzers (MCAs), and the Poynting
flux analyzer (PFX). The plasma wave instrument (PWI) [3],
[4], aboard GEOTAIL, which was designed to observe plasma
waves in the geomagnetic tail, was equipped with sweep
frequency analyzers (SFA), MCAs, and waveform capture
(WFC) receivers. The AKEBONO and GEOTAIL plasma wave
observations have contributed greatly to the progress of mag-
netosphereic plasma physics. The first Japanese Mars orbiter,
NOZOMI (PLANET-B) is now in its heliocentric orbit to arrive
at Mars in early 2004. The low-frequency analyzer (LFA) [5],
onboard NOZOMI, has newly designed digital plasma wave
receivers that include digital filters and fast Fourier transforms
(FFTs) by a central processing unit (CPU) and a digital signal
processor (DSP).

One of the important problems on such spacecraft and plan-
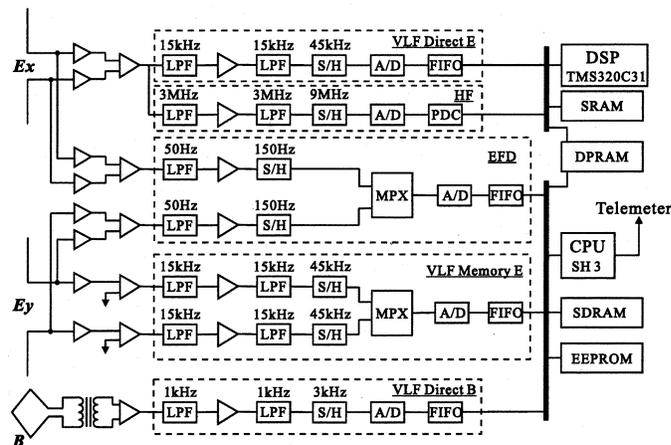etary probes is the transmission to the ground of the data ob-

served in space. Plasma wave instruments, especially waveform
receivers require, huge amounts of data due to the sampling the-
orem. Reasonable telemetry allocations make it almost impos-
sible to transmit all of data to the ground. Other issues in receiver
designs are the restrictions of power, space, and weight in the
spacecraft constrained by the launch capability of the rockets.

To overcome these problems, we have developed a software
wave receiver that mainly consists of a CPU and a DSP. This is
an extension of the LFA and can obtain and transmit observed
data efficiently by performing the onboard signal processing of
signals received by an antenna after they have been converted
into digital data. Conventional plasma wave receivers mainly
consist of analog devices. It is possible to change the character-
istics of the software wave receiver by rewriting the software for
the DSP or CPU. This is a sharp contrast to the hard-wired ob-
servation capability of the conventional receivers. Furthermore,
the volume, power, mass, and cost of the software wave receiver
are much lower than those of conventional ones.

The present paper describes a software wave receiver that
was successfully used in the plasma wave instrument for the
SS-520-2 rocket experiment. The required data rate of the wave-
form receiver was much larger than the telemetry rate allocated
to it. In order to meet the requirement, a new real-time data com-
pression technique was used. This made multichannel waveform
observations possible under the limited telemetry rates. Another
objective was to obtain wideband wave spectra with very high
time and frequency resolutions. It is difficult to achieve them
using the conventional spectral receivers like a sweep frequency
analyzer. We have developed a digital SFA for spectral observa-
tion using a programmable down converter (PDC). Since both

TABLE I
SPECIFICATIONS OF THE PWA

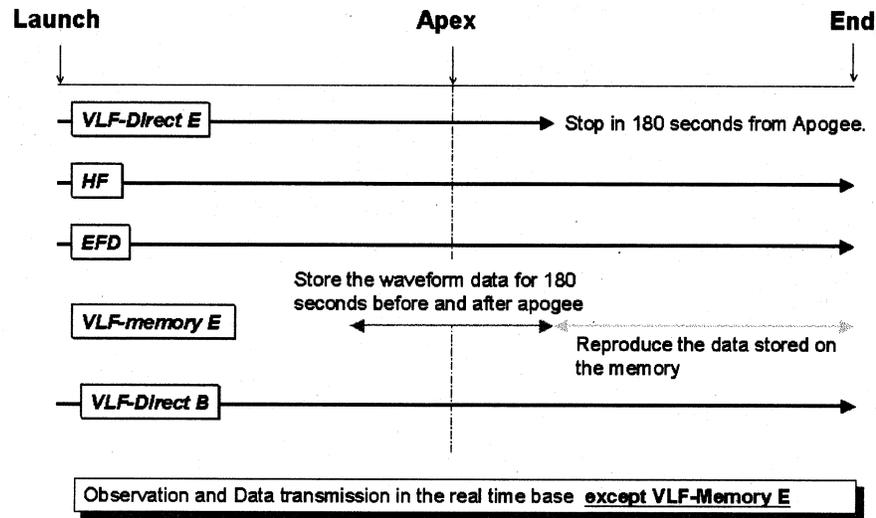| Name of receiver	Frequency range	A/D Sampling rate	A/D resolution	Bit rate(bps) Without compression	Bit rate(bps) With compression
VLF Direct-E	10Hz-15kHz	45kHz	16bits	720,000	~180,000
VLF Memory-E	10Hz-15kHz	45kHz	16bits	1,440,000	~360,000
VLF Direct-B	1Hz-1kHz	3kHz	14bits	42,000	24,000
EFD	0Hz-50Hz	150Hz	16bits	4,800	-
HF	10kHz-3MHz	9MHz	14bits	27,031	-
total	-	-	-	2,233,831	~595,831

Fig. 2. Observation diagram of the PWA onboard the SS-520-2 rocket [12].

SFA and MCA functions are important for the spectrum observation, very high time and frequency resolutions have been attained compared with those of GEOTAIL. Iwai *et al.* [6] give an outline of the PDC and the performance of the digital sweep frequency receiver.

II. SS-520-2 ROCKET EXPERIMENT

The SS-520-2 rocket, whose main objective was to identify the ion acceleration and heating mechanism in the polar cusp region, was launched at 9:16 UT on December 4, 2000, from Ny-Alesund in Svalbard, Norway, at an elevation angle of 86° and an azimuth of 192°. The rocket launch was successful, and it reached its apex of 1108 km at about 601 s after launch and splashdown at about 1150 s after launch. The rocket passed near the cusp.

In order to observe the cusp, the launch timing was decided based on the interplanetary magnetic field (IMF) and solar wind conditions observed by the ACE spacecraft, and the EISCAT radar data on a semi-real-time basis.

A. Objectives of Plasma Wave Observations in the Polar Cusp

In earth's polar cusp, heavy-ions, mainly consisting of oxygen ions, are observed, which flow out from the ionosphere to the magnetosphere and are heated in the perpendicular direction relative to the geomagnetic field. Because the heavy-ions are normally constrained by the earth's gravity, some specific

TABLE II
SPECIFICATIONS

Components	Type	Company	Note
CPU	SH-3(SH7708R)	Hitachi	60MHz
DSP	TMS320C31	TI	50MHz
PDC	HSP50214B	Intersil	9MHz
SRAM	HM628511H	Hitachi	4M × 8bits (× 4)
DPRAM	IDT7016	IDT	16k × 9bits (× 2)
SDRAM	HM5212165H	Hitachi	16M × 8bits (× 4)
EEPROM	HN58V1001FP	Hitachi	128k × 8bits (× 4)
FIFO	IDT72245LB	IDT	4k × 18bits

acceleration and heating mechanisms by wave–particle interactions are required.

Some spacecraft and rockets such as AKEBONO, DE-2 [7], FAST [8], and SCIFER [9]–[11] have made observation in or near the polar cusp region, and particle data and wave spectral data have been obtained. From these observed data, it is speculated that the mechanism starts to work at altitudes above around 1000 km, and that the mechanism relates to the broadband low-frequency waves in the frequency ranges of the lower hybrid waves or the electrostatic ion cyclotron waves. However, no waveform observations have been reported on these spacecrafts and rockets. Although SCIFER was equipped with an waveform observation instrument, the waveform data have not yet been published. The generation mechanism of the broadband low-frequency wave and the detailed relation to the ion heating and acceleration mechanisms have not yet been determined.
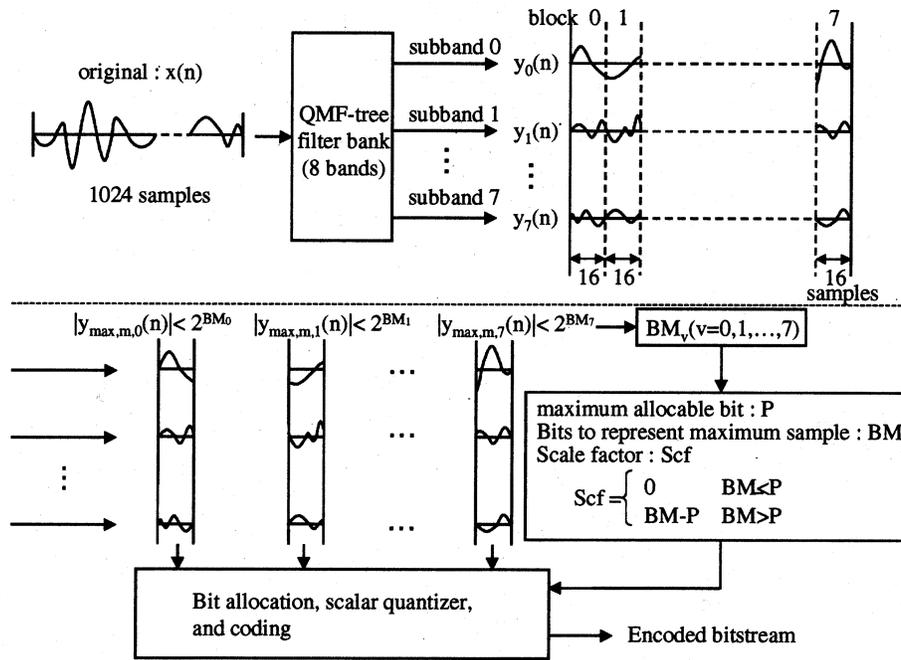
Fig. 3.   Block diagram of a data compression algorithm by subband coding.

In the rocket experiment, the waveform observations are made with a fast analog/digital (A/D) converter. In order to analyze the plasma waves in detail, waveforms of the broadband low-frequency waves are necessary. Actually, some plasma wave phenomena such as electrostatic solitary waves (ESW) have been discovered from the WFC data of the GEOTAIL spacecraft [4]. In the SS-520-2 rocket experiment, it was expected that the waveform data to elucidate the ion acceleration and heating mechanism would be obtained.

This rocket experiment also has the engineering objectives besides the above-mentioned scientific objectives. The engineering objectives are to develop and examine the new plasma wave receivers for the future planet explorers and space observation missions. The plasma wave analyzer (PWA) on this rocket includes the waveform receiver using real-time data compression and the spectral receiver using PDC besides the conventional receivers. These sophisticated receivers will provide us with important plasma wave data for identifying the ion acceleration and heating mechanism.

B. PWA Onboard the SS-520-2 Rocket

By using the results of some spacecraft and rockets that have made observations in or near the polar cusp region, we can assume that the maximum electron density is $n_e = 5 \times 10^4/\text{cm}^3$ in the polar cusp region. From this assumption, the electron, proton, and oxygen plasma frequencies are as follows: $f_{p_e} = 2.0$ MHz, $f_{p_{H+}} = 47$ kHz, and $f_{p_{O+}} = 11.7$ kHz. The electron, proton, and oxygen cyclotron frequencies are as follows: $f_{c_e} = 1.1$ MHz, $f_{c_{H+}} = 600$ Hz, and $f_{c_{O+}} = 37$ Hz. The PWA consists of waveform receivers and a spectral receiver that make observations in the plasma and cyclotron frequency ranges of the ions and electrons, respectively.

A block diagram of the PWA instrumentation is shown in Fig. 1. The PWA has four wire antennas (WANT), each 5 m

long, for the electric field measurements and a ten-turn trapezoidal loop antenna with an area of 1060 cm^2 for the magnetic field measurement. The four wire antennas are used as a 10-m tip-to-tip dipole antenna and a pair of monopole antennas. The PWA consists of three VLF receivers, the electric field detector (EFD), and the high-frequency (HF) receiver. The three VLF receivers are VLF-Direct E, VLF-Memory E, and VLF-Direct B. The VLF-Direct E observes the x component of the electric field E_x with the dipole antenna. The VLF-Memory E observes the y component of the electric fields E_{y_1} and E_{y_2} with the pair of monopole antennas. The VLF-Direct B observes the magnetic field with the loop antenna. The EFD observes the DC electric field, and the HF observes the broadband spectrum of the electric field. All of these receivers, except the HF, are the waveform receivers. The frequency range, sampling frequency, resolution, and bit rate of each receiver are shown in Table I.

Since the amounts of waveform data from VLF-Direct E, VLF-Memory E, and VLF-Direct B are very large, these data are compressed. In the observation of VLF-Direct E and VLF-Memory E, the lossy data compression by subband coding described in Section III-A is used. The volume of these data is compressed at least by a factor of three by this algorithm. In the observations of VLF-Direct B, the μ-CODEC algorithm is used. The 14-bit data are compressed into eight-bit data by this algorithm. The bit rate allocated to the PWA was 300 kb/s. Even with the data being compressed, it was impossible to make the observations and transmit all of the data in real time. In order to overcome this problem, we decided on the observation plan of the PWA as shown in Fig. 2. The sizes of the EFD, HF, and VLF-Direct B datasets were relatively small. Therefore, observations from these receivers were made in real time from launch until the end of the flight. The VLF-Direct E starts the observations at launch and transmits the data to the ground in real time, until 180 s after the apex when it stops. The VLF-Memory E

Scale factors

block 0   1   7

| Scf | Scf | · · · · · | Scf |

4bits 4bits   4bits

Allocated Bits

block 0   block 1   block 7

| B$_0$ | B$_1$ | · · · | B$_7$ | | B$_0$ | B$_1$ | · · · | B$_7$ | · · · · · | B$_0$ | B$_1$ | · · · | B$_7$ |

3bits3bits   3bits

Compressed Samples

block 0   block 1   block 7

| S$_{n0,15}$ | S$_{n1,15}$ | · · · | S$_{n7,15}$ | | S$_{n0,15}$ | S$_{n1,15}$ | · · · | S$_{n7,15}$ | · · · · · · | S$_{n0,15}$ | S$_{n1,15}$ | · · · | S$_{n7,15}$ |

16 samples

| S$_{n0,1}$ | S$_{n1,1}$ | · · · | S$_{n7,1}$ | | S$_{n0,1}$ | S$_{n1,1}$ | · · · | S$_{n7,1}$ | | S$_{n0,1}$ | S$_{n1,1}$ | · · · | S$_{n7,1}$ |
| S$_{n0,0}$ | S$_{n1,0}$ | · · · | S$_{n7,0}$ | | S$_{n0,0}$ | S$_{n1,0}$ | · · · | S$_{n7,0}$ | | S$_{n0,0}$ | S$_{n1,0}$ | · · · | S$_{n7,0}$ |

B$_0$ bits B$_1$ bits   B$_7$ bits

Final Structure of the Encoded Bitstream

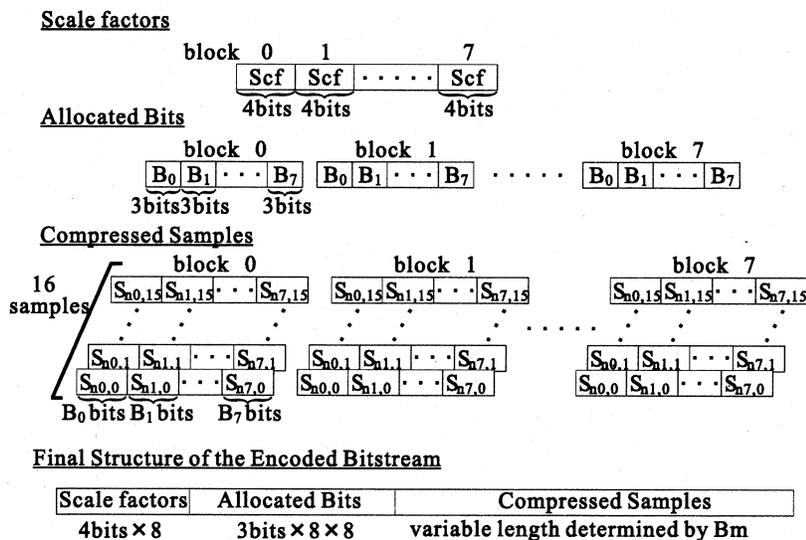| Scale factors	Allocated Bits	Compressed Samples
4bits × 8	3bits × 8 × 8	variable length determined by Bm

Fig. 4. Structure of the encoded bitstream.

only makes observations and stores the waveform data into the onboard memory for 180 s before and after the apex, the most important period of the observation time in this rocket experiment. Beginning 180 s after the apex, the data stored in the memory are reproduced and compressed. The compressed data are transmitted to the ground until the end of the flight. The staggering of the transmission periods for the data from VLF-Direct E and VLF-Memory E made possible to overcome the problem caused by the restriction of the telemetry.

III. SOFTWARE WAVE RECEIVER IN THE SS-520-2 ROCKET EXPERIMENT

In the waveform observations of VLF-Direct E and VLF-Memory E, the lossy data compression by subband coding was used. The HF is the digital sweep frequency receiver using PDC. The digital signal processing was done on the DSP. Since it was necessary to perform high-level digital signal processing, we used the high-performance devices shown in Table II.

A. VLF-Direct E and VLF Memory E

In order to maximize the scientific return of the waveform observations, efficient onboard data compression was necessary. A lossy data compression technique by subband coding [13], [14] was proposed. This technique was adopted for the experiment since real-time data compression was required. This method is based on the techniques based on the MASCAM system [15] and MPEG Audio [16]. However, psychoacoustics was not used, since characteristics of human ears could not be applied.

Fig. 3 shows a block diagram of the lossy data compression algorithm by the subband coding. Since the processing time for data compression was restricted on the SS-520-2 rocket experiment, the number of subband was eight, and the taps of QMF was 16. First, the quadrature mirror filter (QMF)-tree filter bank divides the input samples into eight equal-bandwidth subbands. For every 1024 input samples, the filter bank produces 128 output samples per subband. A block is defined by grouping 16 samples from each of the eight subbands. There are eight blocks in each of the eight subbands, as shown in

Fig. 3. $BM_m (m = 0, \ldots, 7)$ is defined as the number of bits to represent a maximum sample in a block for each subband, and BM is the maximum of BM_m. $P(= 6)$ is defined as the number of maximum allocable bits. A scale factor Scf is given by the following equation:

$$\text{Scf} = \begin{cases} 0 & BM \le P \\ BM - P & BM > P \end{cases}. \quad (1)$$

The number of bits required to represent Scf is four bits per block, since the resolution of the A/D converter is 16 bits. The allocated bits of each subband are given by

$$B_m = BM_m - \text{Scf} \quad (0 \le B_m \le 7). \quad (2)$$

The number of bits required to represent B_m is three bits per subband in a block. Each subband sample $S_{m,i}$ ($m = 0, \ldots, 7$, $i = 0, \ldots, 15$) is normalized with Scf to

$$Sn_{m,i} = 2^{\text{Scf}} S_{m,i}. \quad (3)$$

Equations (1)–(3) are calculated for each of eight blocks. Each subband sample in each block is quantized by a scalar quantizer according to the allocated bit B_m and then an encoded bitstream is produced. The structure of the encoded bitstream is shown in Fig. 4.

VLF-Direct E: The VLF-Direct E observes the waveform in real time over the frequency range from 10 Hz to 15 kHz of the electric field from the *x* component of the WANT dipole antenna. In order to guarantee the frequency range, the sampling rate of the A/D converter is 45 kHz, and its resolution is 16 bits. In order to keep a continuous waveform, a first-in/first-out (FIFO), whose size is 4 k × 18 bits, is used between the A/D converter and the DSP. The reset of the FIFO, which determines the start of the observation of VLF-Direct E, is done by the DSP, after the DSP gets the "FIFO RESET" status from the CPU through the DPRAM. The DSP watches the half-full flag of the FIFO in order not to overflow the FIFO. When the Flag becomes active, 2048 samples on the FIFO are transferred to the external SRAM through the direct memory access (DMA) controller. The DMA controller can read from or write to any
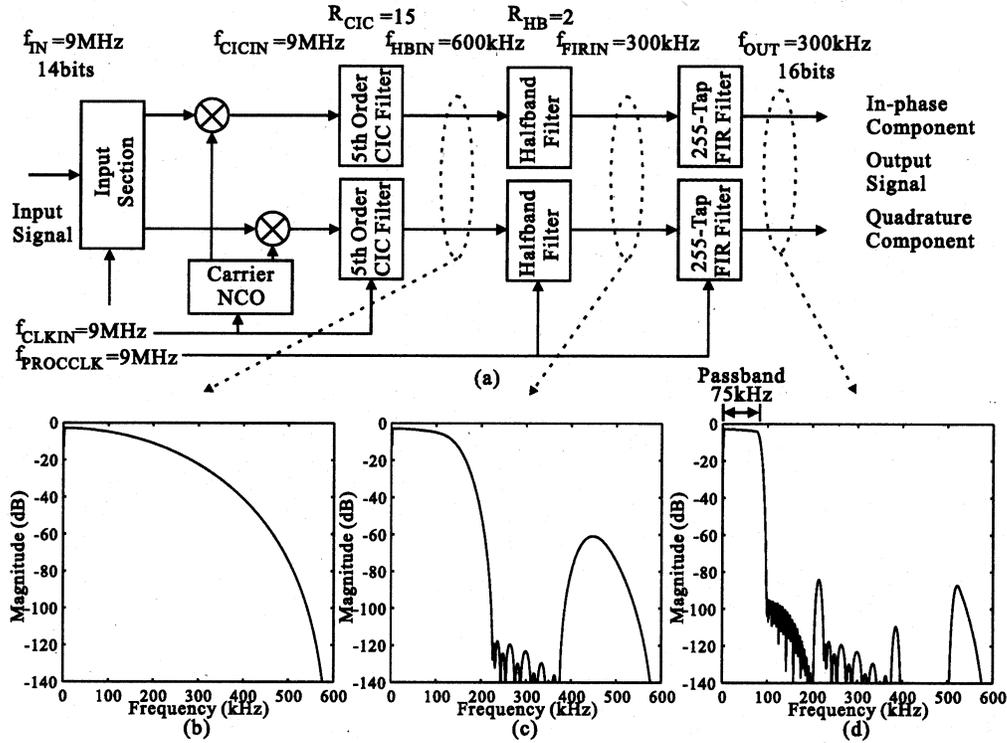
Fig. 5.   (a) Block diagram of PDC and frequency response of PDC. (b) CIC filter response. (c) CIC filter and Halfband filter response. (d) Composite filter response.

locations in the memory map without interfering with the operation of the DSP [17]. Due to the DMA controller, the data compression and the 2048 samples transfer can be performed in parallel. The compressed data are delivered to the CPU through the DPRAM.

VLF-Memory E: The VLF-Memory E observes the waveform over the frequency range from 10 Hz to 15 kHz of the electric field with the *y* components of the WANT monopole antennas. The same types of A/D converter and FIFO as the VLF-Direct E are used. The reset and control of the FIFO are done by the CPU. Because the amount of data of VLF-Memory E is two times as large as that of VLF-Direct E, the waveform data are stored into the SDRAM for 180 s before and after the apex by the CPU. After the observation of VLF-Direct E stops, data from the two components of the monopole antennas E_{y_1} and E_{y_2} are delivered from the CPU to the DSP through the DPRAM. After the data are compressed by the DSP, the compressed data are returned to the CPU through the DPRAM.

B. HF

The HF observes the spectrum in real time over the frequency range from 10 kHz to 3 MHz of the electric field with the *x* component of the WANT dipole antenna. The broadband signal sampled with a frequency of 9 MHz are down-converted into the narrow band signal whose sampling rate is 300 kHz by the PDC. The block diagram of the PDC [18] is shown in Fig. 5(a). This system design was inspired by the introduction of a digital down converter, such as HSP50016 [19]. The PDC was designed from this capability.

TABLE III
FIR FILTER CONFIGURATION

Decimation	1
Passband	75kHz
Transition Band	22.5kHz
Passband Attenuation	0.1dB
Stopband Attenuation	90dB
FIR Order	49
FIR Symmetry	Odd

R_{CIC}, the decimation factor of the cascaded integrator-comb (CIC) filter, was set to 15 and R_{HB}, the decimation factor of the Half Band filter, was set to 2. In order to decrease the power consumption of PDC, the processing clock $f_{PROCCLK}$ has been decreased to 9 MHz to be the same as the input clock f_{CLKIN}. For the generic finite-impulse response (FIR) filter configuration, we used (4) to calculate the number of taps available at the FIR input sample rate f_{FIRIN} and $f_{PROCCLK}$ [18], [20].

$$\text{Taps} = \left(\text{floor} \left[\frac{f_{PROCCLK}}{\left(\frac{f_{FIRIN}}{R} \right) - R} \right] \right)(1 + \text{SYM}) - (\text{SYM} \cdot \text{ODD})$$

(4)

where floor[] is defined as the integer portion of a number; R = decimation rate; SYM = 1 for symmetrical filter, 0 for asymmetrical filter; ODD = 1 for an odd number of filter taps, 0 = an even number of taps. In the rocket experiment, $f_{PROCCLK} = 9$ MHz, $f_{FIRIN} = 300$ kHz, R = 1, SYM = 1, ODD = 1, and Taps = 57. We designed a linear-phase FIR filter using the Parks–McClellan algorithm [21, Alg. 5.1], which

TABLE IV
DATA POINTS AND FREQUENCY RESOLUTION AT EACH FREQUENCY BAND

Band Number	Frequency range(kHz)	Data points	Frequency resolution(kHz)
1	0 - 150	256	0.59
2	150 - 300	128	1.17
3,4	300 - 600	64($\times$2)	2.34
5,6,7	600 - 1050	32($\times$3)	4.69
8 - 20	1050 - 3000	16($\times$13)	9.38
total	-	816	-

Fig. 6.   Digital sweep frequency method.

(1) The 2048 samples are stored into the FIFO.
(2) The DMA transfer begins.
(3) The 1024 samples are compressed. ··· VLF-Direct E or VLF-Memory E
(4) The output of the PDC are converted into spectral data. ··· HF
(5) The data generated at (3) and (4) are delivered to the CPU through the DPRAM.
(6) The waiting time

Fig. 7.   The processing time on the DSP.

is sometimes called equiripple filters. The FIR filter is configured as shown in Table III. The frequency responses of the PDC are shown in Fig. 5(b)–(d).

The 512 inphase and quadrature components of the output of the PDC are fed to the DSP, and converted into the 256 spectral samples by the DSP using the FFT. This processing is performed for each frequency band shown in Table IV and the digital sweep frequency method is shown in Fig. 6. Since it is necessary to reduce the amount of data because of the restriction of the telemetry and the frequency resolution at higher frequency band may be coarse, the data points are changed band by bands. When the data points are 128, 64, 32, and 16, the 256 spectral samples are averaged with 2-, 4-, 8-, and 16-point samples, respectively. The spectral data is an eight-bit integer format data, the resolution of the data is 0.5 dB, and the range of the data is from 0 dB to −127.5 dB. The spectral data and the band number shown in Table IV are transferred to the CPU through the DPRAM.

C. Data Processing

When the VLF-Direct E and HF make observations in parallel, their processing on the DSP is performed in turn as shown in Fig. 7. When the half flag of the DPRAM becomes active, the DMA begins to transfer 2048 samples on the FIFO to the external SRAM. Then the samples on the SRAM that are the previously transferred data by the DMA controller are compressed, and the output of the PDC are converted into the spectral data.
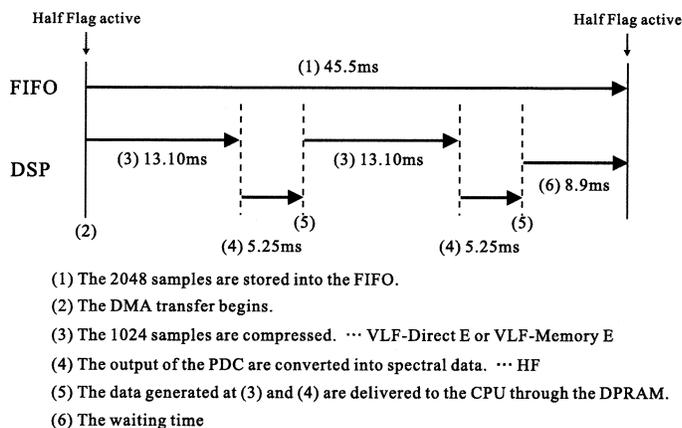
The times for the processing are 13.10 ms and 5.25 ms, respectively. Those times are estimated using the evaluation system. The processing is performed in turn, and then the processing is waiting until the half flag becomes active. The waiting time is about 8.9 ms. The sweep time period of the HF is estimated to be about 455 ms.

When the VLF-Memory E and HF require processing in parallel, their processing on the DSP is performed in turn. In this case, it is not necessary to consider the time when the 2048 samples are stored into the FIFO. The sweep time period of the HF is estimated to be less than 400 ms.

The time resolution of the GEOTAIL MCA is 0.25 or 0.5 s [3]. On the other hand, the frequency resolution is ±7.5% of each center frequency at more than 10 kHz and very wide. The frequency resolution of the SFA is 680 Hz and 5.4 kHz for 12.5–100 kHz and 100–800 kHz, respectively, and the time resolution is 8 s. Compared with those of GEOTAIL, the present system obtains high frequency and time resolution as shown in Table IV within less than 0.5 s. The 12-bit digital data of the A/D converted wave forms obtained by the WFC are compressed into eight bits by a simple hardware quasilogarithmic compression.

IV. EVALUATION OF SOFTWARE WAVE RECEIVER
ON THE ROCKET EXPERIMENT

The PWA operated flawlessly and very good data of VLF-Direct E, VLF-Memory E, and HF were obtained.

Fig. 8 shows the frequency-time spectrogram observed by the HF. "TIME" and "ALT" in Fig. 8 are the time from the launch and the altitude, respectively. The time range from 200–1100 s is from the completion of the WANT deployment to the splashdown. At the frequency around 10 kHz, we see auroral hiss that is a continuous wideband noise and is observed over the whole polar cap [22].

As mentioned in the preceding section, when the VLF-Direct E and HF make observation in parallel, the sweep time period of the HF is estimated to be about 455 ms. On this observation the sweep time fluctuated and there were cases where the sweep time exceeded 455 ms. This "data jam" occurs when the size of data on the DPRAM is larger than the size of transferable data allocated for the telemetry for a given time. Since a waiting time is necessary to write the next data to DPRAM, the sweep
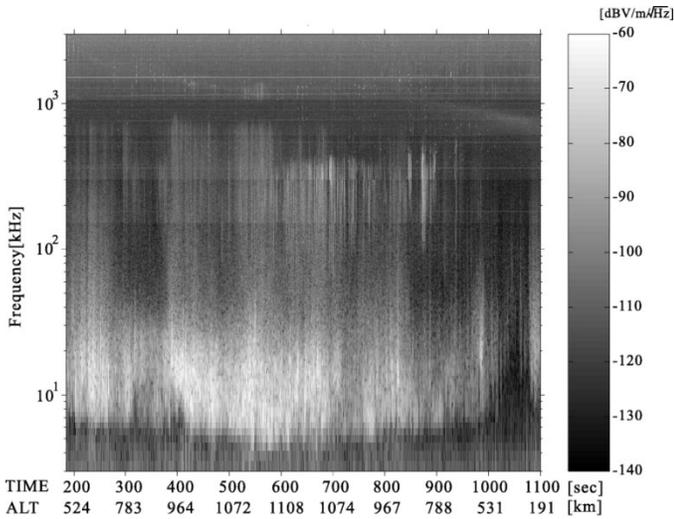
Fig. 8.   Frequency-time spectrogram observed by the HF.

Fig. 9.   Frequency-time spectrogram observed by the VLF-Direct E.

time exceeds 455 ms. When the VLF-Memory E and HF make processing in parallel, the sweep time period of the HF is estimated to be below 400 ms. During these observations the sweep time also fluctuated and there were cases where the sweep time exceeded 400 ms. In this case, this is also caused by the data jam. The data jam occurs when data happen to be compressed less than expected. This, however, caused no loss of data in the flight.

The waveform data of the VLF-Direct E and the VLF-Memory E were reconstructed from the compressed data on the ground. The amplitude of the waveform data was calibrated. A frequency-time spectrogram shown in Fig. 9 was made from the waveform data observed by the VLF-Direct E using the Fourier transform. The VLF-Direct E stopped at about 770 s into the flight on schedule. Although there were a few data losses caused by telemetry error, no data loss was caused by the overflow of the FIFO. The processing of VLF-Direct E and HF on the DSP, which is shown in Fig. 7, worked very well. It was confirmed that the volume of the waveform data was compressed by a factor of four by this algorithm

The frequency-time spectrograms shown in Fig. 10 are made from the waveform data observed by the VLF-Memory E using the Fourier transform. Fig. 10(a) and (b) are the y components of the electric fields, E_{y_1} and E_{y_2}, respectively. The VLF-Memory E started at about 410 s on schedule, and then made observations until about 770 s. The data observed from 410 s to about 600 s were able to be transmitted to the ground by the end of flight. Since the amount of the data observed by VLF-Memory E for 360 s is mostly equal to the amount of the data observed by VLF-Direct E for 720 s, it should take about 720 s to transmit the overall observed data. Because the time to transmit the data was about $330 (= 1100 - 770)$ s, slightly less than half the amount of the observed data were transmitted.

In Figs. 9 and 10, hiss at a frequency around 10 kHz is observed similar to the HF results. There is also a very strong wideband noise band in the frequency range from 10–100 Hz.

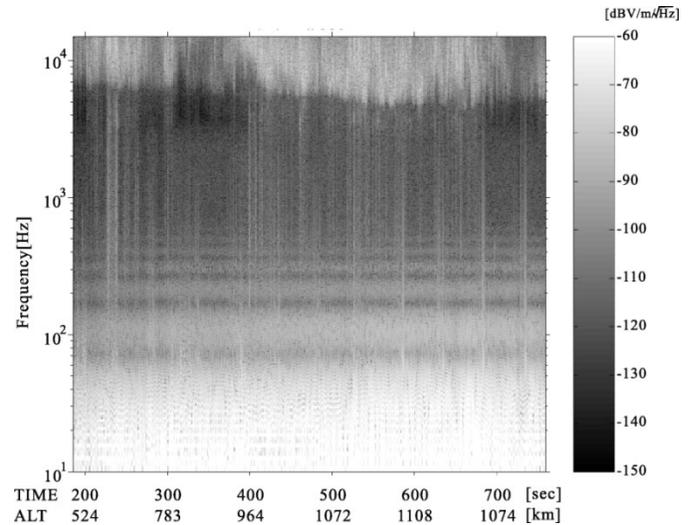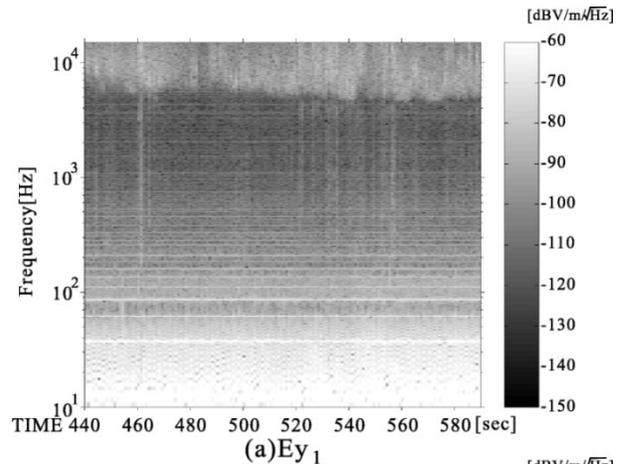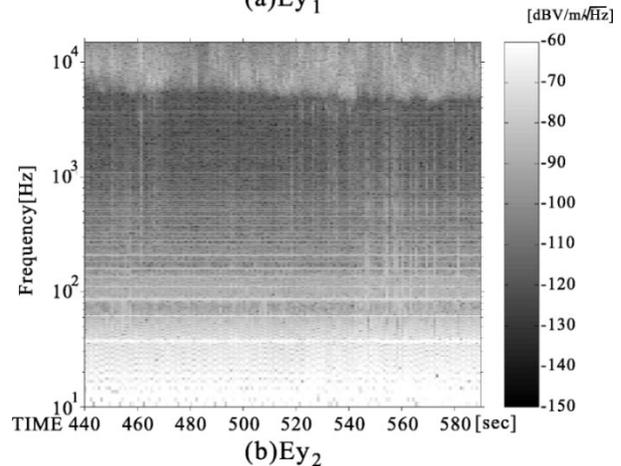Fig. 11 shows the waveforms of the VLF-Direct E and the VLF-Memory E for a period of about 1 s beginning at 460 s.

(a)Ey$_1$

(b)Ey$_2$

Fig. 10.   Frequency-time Spectrogram observed by the VLF-Memory E; (a)E_{y_1}, (b)E_{y_2}.

Fig. 12 shows the frequency-time spectrograms made from these waveform data. In Fig. 11(a), there are very strong bipolar pulse-like noises at about 460.15, 460.5, and 460.85 s. In Fig. 11(b) and (c), there are similar noises at about 460, 460.35, and 460.7 s. The very strong wideband noises in the frequency range from 10–100 Hz in Fig. 12(a)–(c), are consistent with
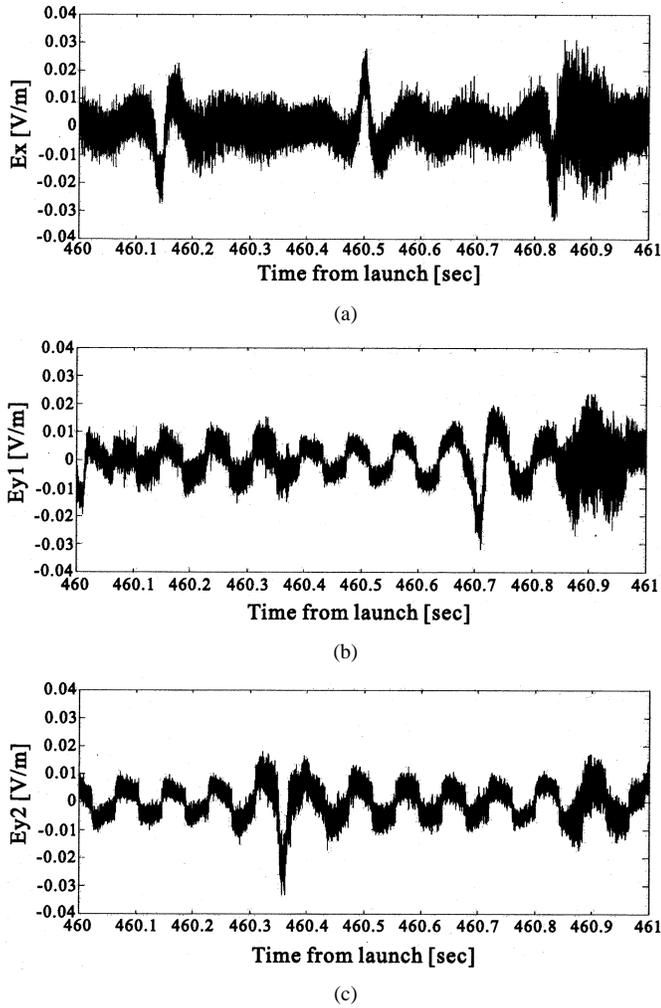
Fig. 11. Waveforms of the VLF-Direct E and VLF-Memory E for a period of about 1 s after 460 s; (a)VLF-Direct E, (b)VLF-Memory E E_{y_1}, (c)VLF-Memory E E_{y_2}.

Fig. 12. Frequency-time spectrograms of the VLF-Direct E and VLF-Memory E from 460 to 461 s; (a)VLF-Direct E, (b)VLF-Memory E E_{y_1}, (c)VLF-Memory E E_{y_2}.

the very strong bipolar pulse-like noises. This noise has the following characteristics.

1) The difference of the phase between the noise in Fig. 11(a), and the noise in Fig. 11(b) and (c) is about 90° difference in the antenna directions.
2) In Fig. 11(b) and (c), the polarity of the noise is the same on each monopole antenna.
3) In Fig. 11(b), the period of the noise received by a monopole antenna is about 0.7 s.

Since the rocket spin period is about 1.5 rotations per second, which is about 0.7 s per rotation, it is consistent with the period of the noise received by a monopole antenna. The potential of an element of a dipole antenna or a monopole antenna is increased by the photo-electron emissions due to solar irradiation. Shading from the rocket body causes a change of the potential and creates this spiky noise [3].

The wave spectrum from 461–462 s and waveform in the frequency range of 3–4 kHz are shown in Fig. 13 [23]. The emissions above 6 kHz are auroral hiss, and another peak exists around 3–4 kHz in the spectrum. The observed waveforms in the latter frequency range show the impulsive waveforms. The waveforms appear in a short duration of time and their frequency
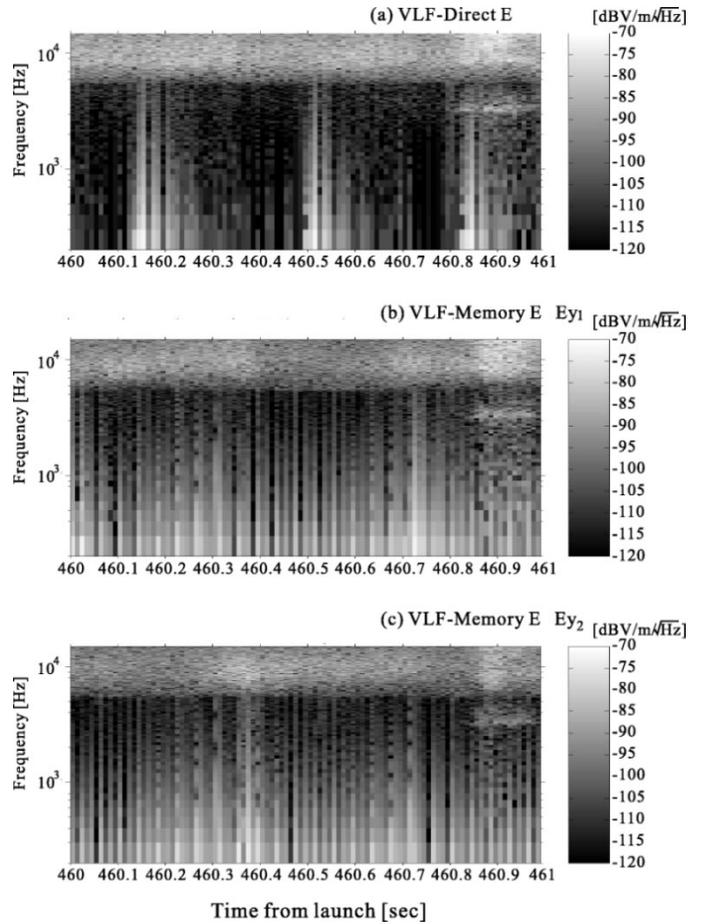
spectral peaks are well below the lower cut off frequency of the auroral hiss emission. Their polarizations are almost linear determined by the two sets of orthogonal wire antennas lying on the rocket spin plane that is almost perpendicular to the ambient magnetic field. The local lower hybrid frequency is estimated to be 3–6 kHz corresponding to the local proton population of 5% to 10%. The most plausible wave mode is the quasi-electrostatic lower hybrid wave. The PWA has the capability to identify the wave propagation direction and to estimate corresponding phase velocity by the onboard interferometry system using a pair of the monopole antennas E_{y_1} and E_{y_2}. From the cross correlation in the interferometry system, we can roughly estimate the phase velocity of the wave to be almost 60 km/s. We have also conducted the linear dispersion analyses using realistic parameters that show that electron beam can destabilize the electrostatic waves around the lower hybrid frequency.

V. SUMMARY AND DISCUSSION

The software wave receiver was used on the SS-520-2 rocket experiment and has successfully provided high time and frequency resolution data. The ion acceleration and heating mechanism in the polar cusp region will be studied through the analysis of those data. Furthermore, the success of the rocket experiment
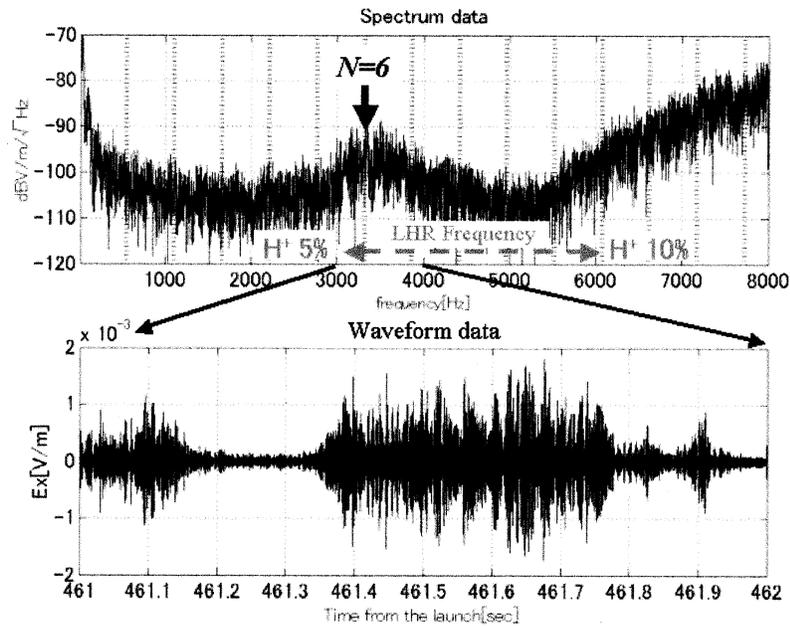
Fig. 13. Frequency spectrum and waveform of the VLF-Direct E from 461–462 s. (Top) Spectrum. (Bottom) Waveform.

shows the practicality of the software wave receiver, and we expect that this receiver will contribute greatly to the progress of plasma wave observations on future planet explorer and space observation missions.

On this rocket experiment, there were some problems identified and items found that need to be improved. When the data compression of the VLF-Direct E and VLF-Memory E was performed, the compressed datasets were large, and the "data jam" occurred. Although there were a few data losses caused by the telemetry errors during the observation of the VLF-Direct E, no data loss was caused by the overflow of the FIFO. The data jam could have been avoided if we had designed the receiver at lower expected compression ratio, but the present design would still be better, since there was no data loss. For the observations from VLF-Memory E, about half the amount of the observed data were able to be transmitted to the ground as we had expected. There was no problem as regards to the processing time of the data compression. The data jam influenced the sweep time of the HF. When the VLF-Direct E and HF made observations in parallel, the sweep time fluctuated, and there were cases where the sweep time exceeded 455 ms. When the VLF-Memory E and HF did processing in parallel, the sweep time also fluctuated, and there were cases where the sweep time exceeded 400 ms.

The waveform observation clarified that very strong bipolar pulse-like photo-electron emissions were included in the waveform data observed by the VLF-Direct E and VLF-Memory E. Some impulsive waves were analyzed, and their mode has been identified. The phase velocity has been estimated using the two monopole antennas [23].

The software wave receiver will also be aboard SELENE and is named WFC. The hardware of the WFC is based on that of the VLF-Direct E and HF used on the rocket experiment. We expect that the WFC will provide us with as fruitful data as the PWA did aboard the SS-520-2 rocket.

REFERENCES

[1] K. Hashimoto, I. Nagano, M. Yamamoto, T. Okada, I. Kimura, H. Matsumoto, and H. Oki, "EXOS-D(AKEBONO) very low frequency plasma wave instruments(VLF)," IEEE Trans. Geosci. Remote Sensing, vol. 35, pp. 278–286, Mar. 1997.
[2] I. Kimura, K. Hashimoto, I. Nagano, T. Okada, M. Yamamoto, T. Yoshino, H. Matsumoto, M. Ejiri, and K. Hayashi, "VLF observations by the Akebono(EXOS-D) satellite," J. Geomag. Geoelectr., vol. 42, pp. 459–478, 1990.
[3] H. Matsumoto, I. Nagano, R. R. Anderson, H. Kojima, K. Hashimoto, M. Tsutsui, T. Okada, I. Kimura, Y. Omura, and M. Okada, "Plasma wave observations with GEOTAIL spacecraft," J. Geomag. Geoelectr., vol. 46, pp. 59–95, 1994.
[4] H. Kojima, "Study on the Plasma Waves in the Geomagnetic Tail Region via Spacecraft Observations," Ph.D. thesis, Faculty of Engineering, Kyoto Univ., Kyoto, Japan, 1998.
[5] H. Matsumoto, T. Okada, K. Hashimoto, I. Nagano, S. Yagitani, M. Tsutsui, Y. Kasaba, K. Turuda, H. Hayakawa, A. Matsuoka, S. Watanabe, H. Ueda, I. Kimura, Y. Kasahara, Y. Omura, T. Matsumura, T. Imachi, K. Ishisaka, and Y. Tateno, "Low frequency plasma wave analyzer (LFA) onboard the PLANET-B spacecraft," Earth Planets Space, vol. 50, pp. 223–228, 1998.
[6] H. Iwai, K. Hashimoto, H. Matsumoto, and H. Kojima, "Development of a software wave receiver onboard spacecraft," IEICE Trans. Commun., 2003, submitted for publication.
[7] S. A. Curtis, W. R. Hogey, L. H. Brace, N. C. Maynard, M. Sugiura, and J. D. Winningham, "DE-2 cusp observations, role of plasma instabilities in topside ionospheric heating and density fluctuations," Geophys. Res. Lett., vol. 9, pp. 997–1000, 1982.

[8] R. Pfaff, J. Clemmons, C. Carlson, R. Ergun, J. McFadden, F. Mozer, M. Temerin, D. Klumpar, W. Peterson, E. Shelley, E. Mœbius, L. Kistler, R. Strangeway, R. Elphic, and C. Cattell, "Initial FAST observations of acceleration process in the cusp," *Geophys. Res. Lett.*, vol. 25, pp. 2037–2040, 1998.

[9] P. M. Kintner, J. Bonnell, R. Arnoldy, K. Lynch, C. Pollock, T. Moore, J. Holtet, C. Deerhr, H.-S. Nielsen, R. Smith, J. Olson, and J. Moen, "The SCIFER experiment," *Geophys. Res. Lett.*, vol. 23, pp. 1865–1868, 1996.

[10] P. M. Kintner, J. Bonnell, R. Arnoldy, K. Lynch, C. Pollock, and T. Moore, "SCIFER—Transverse ion acceleration and plasma waves," *Geophys. Res. Lett.*, vol. 23, pp. 1873–1876, 1996.

[11] T. E. Moore, C. J. Pollock, M. F. Adrian, P. M. Kintner, and R. L. Arnoldy, "SCIFER—The cleft ion plasma environment at low solar activity," *Geophys. Res. Lett.*, vol. 23, pp. 1877–1880, 1996.

[12] Y. Ueda, H. Kojima, H. Iwai, R. Fujiwara, K. Hashimoto, H. Matsumoto, I. Nagano, and T. Okada, "Development of plasma wave analyzer with the digital control system for the rocket experiment in the polar region" (in Japanese), *IEICE Trans. Commun.*, vol. J84–B, pp. 1808–1818, 2001.

[13] A. Suzuki, "Study on intelligent receiver onboard scientific spacecraft and waveform data compression," Bachelor's thesis (in Japanese), Faculty of Engineering, Kyoto Univ., Kyoto, Japan, 1997.

[14] M. Kabeuchi, "High efficiency waveform transmission for plasma wave software receiver onboard a spacecraft," Master's thesis (in Japanese), Dept. of Communications and Computer Engineering, Grad. School of Informatics, Kyoto Univ., Kyoto, Japan, 2000.

[15] G. Theile, G. Stoll, and M. Link, "Low Bit-Rate Coding of High-Quality Audio signals: An introduction to the MASCAM system,", EBU-Review—Tech. Rep. 230, S., 1988.

[16] D. Pan, "A tutorial on MPEG/audio compression," *IEEE MultiMedia*, vol. 2, pp. 60–74, 1995.

[17] Texas Instruments, *TMS320C3x User's Guide*. Dallas, TX: Texas Instruments, July 1997.

[18] Intersil Corporation, "HSP50214B data sheet," Intersil, Milpitas, CA, http://www.intersil.com/data/fn/fn4/fn4450/index.asp, 2000.

[19] R. Baines, "The DSP bottleneck," *IEEE Commun. Mag.*, vol. 33, pp. 46–54, 1995.

[20] Intersil Corporation, "Calculating maximum processing rates of the PDC (HSP50214, HSP50214A and HSP50214B)," Intersil, Milpitas, CA, http://www.intersil.com/Data/AN/AN9/AN9720, 1999.

[21] IEEE, *Programs for Digital Signal Processing*. New York: IEEE Press, 1979.

[22] R. E. Ergun, E. Klementis, C. W. Carlson, J. P. McFadden, and J. H. Clemmons, "Wavelength measurements of auroral hiss," *J. Geophys. Res.*, vol. 96, pp. 21 299–21 307, 1991.

[23] Y. Ueda, H. Kojima, H. Matsumoto, K. Hashimoto, I. Nagano, T. Okada, and T. Mukai, "Lower hybrid waves observed at the dayside polar region: SS-520-2 rocket experiment," *Radio Sci.*, 2003, to be published.

Kozo Hashimoto (SM'86) was born in Kyoto, Japan, in 1947. He received the B.E., M.E., and Doctor of Engineering from Kyoto University, Kyoto, Japan, in 1969, 1971, and 1980, respectively.

From 1974 to 1985, he was with the Department of Electrical Engineering, Kyoto University. From 1981 to 1983, he was an NRC Resident Research Associate at NASA Goddard Space Flight Center, Greenbelt, MD. From 1985 to 1995, he was a Staff Member of the Department of Electrical Engineering, Tokyo Denki University, Tokyo, Japan, where he had been a Professor since 1989. He was a Professor at the Radio Atmospheric Science Center (RASC), Kyoto University from 1995 to 2000. He has been a Professor at RASC for Space and Atmosphere, Kyoto University, since 2000. His research interests include space radio science, especially the theoretical and experimental studies of the plasma wave propagation in the magnetospheres, packet radio networks, satellite communications, and microwave power transmission.

Dr. Hashimoto is a member of Institute of Electronics, Information and Communication Engineers of Japan, the Society of Geomagnetism and Earth, the Planetary and Space Science (SGEPSS) of Japan, and the American Geophysical Union. He was awarded Tanakadate Award, SGEPSS, in 1984.

Hironori Iwai was born in Nagano, Japan, in 1977. He received the Bachelor's degree in electrical and electronic engineering and the Master's degree in informatics, in 1999 and 2001, respectively, both from Kyoto University, Japan.

In 2001, he has joined the Communications Research Laboratory (CRL), Hiraiso Solar Observatory, Ibaraki, Japan, as a Researcher of Solar and Solar Wind Group of Applied Research and Standards Division.

Mr. Iwai is a member of Society of Geomagnetism and Earth, Planetary and Space Sciences.

Yoshikatsu Ueda received the B.E. and M.E. degrees in electronics engineering, in 1997 and 1999, respectively, from Kyoto University, Kyoto, Japan.

Since 2002, he have been working as a Research Associate for the space engineering and science at the Radio Science Center for Space and Atmosphere, Kyoto University. His research interests are in the development of plasma wave observation systems and the hybrid IC design for future microsatellites.

Mr. Ueda is a member of Institute of Electronics, the Information and Communication Engineers of Japan, the American Geophysical Union, and the Society of Geomagnetism and Earth, Planetary and Space Sciences.

Hirotsugu Kojima was born on July 30, 1963, in Shizuoka Prefecture, Japan. He received the B.Eng. degree, the M.Eng. degree, and the Dr.Eng. degree in 1987, 1989, and 1998, respectively, each from Kyoto University, Kyoto, Japan.

Since 1989, he has been with Radio Science Center for Space and Atmosphere, Kyoto University and has been working on plasma wave observations in space via spacecraft and rockets.

Dr. Kojima is a member of Institute of Electronics, the Information and Communication Engineers of Japan, the Society of Geomagnetism and Earth, Planetary and Space Science (SGEPSS) of Japan, and the American Geophysical Union.

Hiroshi Matsumoto (SM'96-F'03) was born in Nara, Japan, in 1942. He received the B.Eng., M.Eng., and Dr.Eng. degrees in 1965, 1967, and 1973, respectively, each from Kyoto University, Kyoto, Japan.

Since 1987, he is Professor at the Radio Science Center for Space and Atmosphere, Kyoto University, and served as its Director from 1992 to 1998, as well as from 2002 to 2004. He was a Visiting Research Scientist at the NASA Ames Research Center, Moffet Field, CA, from 1975 to 1977, and at Stanford University, Stanford, CA, in 1983. He is also a Visiting Professor at the Institute for Space and Aeronautical Sciences (ISAS), Sagamihara, Japan, and the National Institute for Fusion Science, Toki, Japan. His main research interests include space plasma wave research via satellite observations, theory and simulations of nonlinear plasma wave phenomena, microwave power transmission, and its application to solar powered satellites.

Dr. Matsumoto is a member of Institute of Electronics and the Information and Communication Engineers of Japan. He was President of the Society of Geomagnetism and Earth, Planetary and Space Science (SGEPSS) of Japan and is a Fellow of American Geophysical Union. He was President of the International Union of Radio Science (URSI). He was awarded the Shida-Rinzaburo Award in 1999, NASA Group Achievement Awards for GEOTAIL PWI Team for Global Geospace Science (GGS) in 1998, Polar PWI Team for GGS in 1998, GEOTAIL Plasma Wave Instruments in 1993, and the Tanakadate Award, SGEPSS, in 1975.